MATERIALS CHEMISTRY
FRONTIERS

RESEARCH ARTICLE

View Article Online
View Journal

Open Access Article. Published on 25 January 2025. Downloaded on 2/21/2025 12:54:23 PM.
This article is licensed under a Creative Commons Attribution-NonCommercial 3.0 Unported Licence.

Check for updates

Cite this: DOI: 10.1039/d4qm01070a

Enhancing cycling stability of Li-rich Mn-based cathode materials *via* cyano functional additives†

Dongwei Zhou,[a] Zhanlin Yang,[b] Shihao Wang,[a] Guiyang Gao,[a] Jie Zhu,[a] Chengkun Zhang,[a] Saichao Li,[a] Baisheng Sa,[b] Jie Lin,*[a] Dong-Liang Peng*[a] and Qingshui Xie*[a]

Received 7th December 2024,
Accepted 24th January 2025

DOI: 10.1039/d4qm01070a

rsc.li/frontiers-materials

Li-rich Mn-based cathode materials (LRMs) have garnered considerable interest for their high specific capacity. Nevertheless, the elevated operating voltage window presents a great hurdle to the high-voltage tolerance of the conventional electrolytes, and the induced issues such as rapid capacity and structure degradation also further impede their industrial application. In this regard, an efficient method to alleviate this problem is proposed *via* a cyano functional additive. By introducing the trimethylsilyl cyanide (TMS) additive into a carbonate electrolyte to construct a complex with TM–CN bonds on the cathode surface and form a low-impedance and durable cathode/electrolyte interphase (CEI), both electrolyte decomposition and cathode degradation are suppressed effectively. Moreover, harmful substances are also removed through the reaction between TMS and HF to purify the electrolyte. Therefore, the electrochemical performance of the LRM cathode is enhanced with a discharge capacity of 224 mA h g^{-1} after 200 cycles at 1C. A high discharge capacity of 227 mA h g^{-1} is also achieved after 50 cycles at 0.5C under a high mass loading of 13 mg cm^{-2}. This work presents a new path to develop high-voltage electrolytes for LRM cathodes.

1. Introduction

Electric vehicles and other electronic products have flourished in recent decades, and the energy density of lithium-ion batteries needs to be further elevated to meet the development demands of this industry.[1] The use of electrode materials with high specific capacity is crucial for fulfilling this demand. Compared to anode materials, cathode materials are the main bottleneck due to their significantly lower specific capacity.[2,3] Currently, the widely used cathodes such as $LiFePO_4$, $LiTMO_2$ (TM = Ni, Co, and Mn), and $LiCoO_2$ have limited potential for continuously increasing the energy density. Spinel-type lithium nickel manganese oxide has a high operating voltage, but its reversible capacity is too low.[4] In contrast, Li-rich layered cathode materials (LRM, $x\text{Li}_2\text{MnO}_3(1-x)\text{LiTMO}_2$) with ultra-high specific capacity (>300 mA h g^{-1}) and energy density (>1000 W h kg^{-1}) have attracted widespread attention from researchers due to their charge compensation mechanism of additional oxygen anions at high voltage (>4.5 V).[2,5,6] However, a series of challenges such as serious voltage decay, rapid capacity fading, and slow dynamics still hinder their practical commercial applications. The issues are not only related to the intrinsic structural instability of LRMs, but also have a great impact on the deterioration of the surface structure during the charging and discharging process. The high operating voltage window (up to 4.8 V) results in poor compatibility with conventional carbonate electrolytes.[7] Under such harsh conditions, certain undesired reactions may occur intensely on the electrode surface, such as oxidative decomposition of the electrolyte, rupture of the cathode/electrolyte interphase (CEI), erosion of the cathode structure from the surface to bulk, and dissolution of transition metals (TMs) into the carbonate electrolyte. These issues will cause continuous damage to the structural stability of LRMs, ultimately aggravating the above-mentioned problems.[8,9]

To enhance the high-voltage stability of the electrolyte in lithium batteries, various strategies have been proposed, including the use of nitrile-based solvents, sulfone-based solvents, high-concentration electrolytes (HCEs), and ionic liquid electrolytes.[10] However, these approaches often introduce additional challenges concerning ionic conductivity, viscosity, wettability, cost, *etc.*[10,11] The widely used carbonate electrolytes are composed of $LiPF_6$ as the solute, along with cyclic and linear carbonates as the organic solvent. This combination

---

[a] *State Key Laboratory of Physical Chemistry of Solid Surface, Fujian Key Laboratory of Surface and Interface Engineering for High Performance Materials, College of Materials, Xiamen University, Xiamen 361005, China. E-mail: linjie@xmu.edu.cn, dlpeng@xmu.edu.cn, xieqsh@xmu.edu.cn*

[b] *College of Materials Science and Engineering, Fuzhou University, Fuzhou 350108, China*

† Electronic supplementary information (ESI) available. See DOI: **https://doi.org/10.1039/d4qm01070a**

Open Access Article. Published on 25 January 2025. Downloaded on 2/21/2025 12:54:23 PM. This article is licensed under a Creative Commons Attribution-NonCommercial 3.0 Unported Licence.

demonstrates favorable characteristics in terms of electrochemical performance and cost-effectiveness. Therefore, using functional additives to optimize the electrolyte for matching the LRM cathode on this basis is a promising strategy.

Nevertheless, there are still notable concerns regarding carbonate electrolytes. The presence of trace water in the electrolyte and the unsatisfactory stability of $LiPF_6$ often lead to the generation of HF. This acidic compound can accelerate the corrosion on the cathode surface, the dissolution of TMs, and the expansion of microcracks, which deteriorates the electrochemical performance greatly. In this regard, some researchers have used alkane additives with Si–O bonds to mitigate the decomposition of $LiPF_6$ and to remove HF.[6,12] Moreover, some organic substances containing Si–N bonds, such as heptamethyldisilazane (HMDS) and 1-(trimethylsilyl) imidazole (1-TMSI), have shown similar beneficial effects.[13,14] In addition, some organic compounds containing cyano functional groups are also used as electrolyte additives. The cyano-groups with powerful electron-withdrawing properties exhibit high electronegativity and strong coordination ability with TM ions. This allows them to be adhered to the cathode surface effectively and participate in the CEI formation, which helps relieve electrolyte oxidation and suppress TM dissolution.[15,16]

Herein, trimethylsilyl cyanide (TMS) is introduced as a high-voltage additive into the carbonate electrolyte. TMS can be adsorbed on the cathode surface to form a complex with TM–CN bonds due to the presence of the electronegative cyano-group, and also contributes to the formation of a uniform and stable CEI layer, which is beneficial for maintaining the structural stability of LRM cathodes during cycling at high-voltage. Additionally, the Si–C bond in the molecular structure also plays a positive role in removing HF for purifying the electrolyte. The electrochemical tests indicate that the addition of TMS can evidently improve the cycling stability of the LRM cathode. The constructed Li||LRM battery with the TMS additive delivers an impressive reversible capacity of 224 mA h g^{-1} at 1C between 2 and 4.8 V with a 91% capacity retention after 200 cycles, which is much higher than that (68%) of the baseline electrolyte after 150 cycles. In addition, the Li||LRM battery with the TMS additive also exhibits better performance at high mass loading and low (−15 °C) and high temperatures (45 °C). This simple approach can simultaneously improve the cathode interface stability and remove the HF residuals, which provides a new pathway for developing high-voltage LRM cathodes through electrolyte engineering.

2. Experimental section

2.1. Preparation of LRM cathodes and electrolytes

The Li-rich Mn-based cathode ($Li_{1.2}Mn_{0.54}Ni_{0.13}Co_{0.13}O_2$) was prepared by the co-precipitation method. Initially, certain amounts of transition metal salts (manganese sulfate, nickel sulfate, and cobalt sulfate) were dissolved in ultrapure water in a stoichiometric ratio of 4 : 1 : 1. Then, sodium carbonate and sodium tartrate, which served as the precipitating agent and complexing agent, were mixed with the prepared salt solution under a N_2 atmosphere to achieve the carbonate precursor. The above precursor was heated at 500 °C for 5 hours, and then evenly mixed with an appropriate amount of lithium source. Finally, the target product was obtained after calcining the mixtures at 800 °C for about 10 hours, which was abbreviated as LRM. After that, LRM, PVDF, and acetylene black were dispersed in NMP at a mass ratio of 8 : 1 : 1 to obtain a uniform cathode slurry with continuous stirring. The slurry was then cast onto aluminum foil, punched into disks with a 12 mm diameter after drying for about 12 hours, and finally transferred into an argon-filled glove box. The conventional mass loading of the cathode material was ∼1.5 mg cm^{-2}, and the high mass loading was ∼13 mg cm^{-2}. The electrolytes were prepared in the glove box. The baseline electrolyte was purchased from DodoChem, with 1 M $LiPF_6$ dissolved in a mixture of cyclic and linear carbonates (EC : EMC : DMC = 1 : 1 : 1, wt%). Trimethylsilyl cyanide (TMS) was purchased from Heowns and treated with molecular sieves before use. Then 1 wt%, 2 wt%, 3 wt%, and 5 wt% TMS were added into the baseline electrolyte and named TMS-1, TMS-2, TMS-3, and TMS-5, respectively.

2.2. Electrochemical measurements

Electrochemical tests were performed in coin-type (CR2025) cells with lithium foil as the counter electrode and Celgard 2500 microporous membrane as the separator. Symmetrical batteries were assembled with 2032-type coin cells. All the cells were assembled in a glove box with H_2O and O_2 content below 0.1 ppm. The cells were activated for one cycle at 0.2C (1C = 250 mA h g^{-1}) before charging and discharging tests with different current densities on the Neware battery test system (CT-4008T, Neware Electronics Co., Ltd, China). The linear sweep voltammetry (LSV) test was carried out on a CHI660E electrochemical workstation (Shanghai Chenhua Instrument Corp., China) with a scanning rate of 0.5 mV s^{-1}. Electrochemical impedance spectroscopy (EIS) was performed on a PARSTAT 3000A-DX electrochemical workstation (AMETEK Instrument Corp., USA) with a voltage amplitude of 5 mV at the frequency of 100 K–0.001 Hz. Self-discharge tests were recorded at a voltage of 4.8 V for 240 h after 100 cycles at 1C. Floating charge performance was evaluated at 4.8 V to monitor the level of leakage current after 100 cycles at 1C. Galvanostatic intermittent titration technique (GITT) curves were assessed at 0.2C for 20 minutes followed by a 3 h rest period after 20 cycles. Additionally, the high-temperature property test was conducted at 1C and 45 °C, while the low-temperature property test was performed at 0.33C and −15 °C. Both of them were activated at 0.2C for one cycle before cycling. The *in situ* XRD measurements were conducted by integrating the Neware battery testing channel and the XRD equipment. The battery was assembled with lithium metal as the anode and LRM as the cathode in the specially designed mold, followed by cycling twice at 0.5C in the voltage range of 2–4.8 V. During the whole charging and discharging processes, the LRM cathodes were tested through an automated program, and the real-time change trend of the (003) diffraction peak with voltage recorded in the range of 17.5–19.5°.

This journal is © The Royal Society of Chemistry and the Chinese Chemical Society 2025

Open Access Article. Published on 25 January 2025. Downloaded on 2/21/2025 12:54:23 PM.
This article is licensed under a Creative Commons Attribution-NonCommercial 3.0 Unported Licence.

2.3. Characterization

The cycled electrodes disassembled from the batteries were washed with DMC, followed by drying naturally in the glove box for a series of tests. A scanning electron microscope (SEM, Hitachi SU-70) and a transmission electron microscope (TEM, Talos F200) were used to observe the surface morphologies of the samples. The chemical structures of the samples were characterized using the Raman spectrum (Xplora). *In situ* XRD tests were performed to track the changes of the (003) diffraction peak during the initial charging and discharging process. The structural changes of the cycled electrodes were also analyzed by X-ray diffraction (XRD, Bruker Axs X-ray diffractometer). X-ray photoelectron spectroscopy (XPS, PHI Quantum 2000) was utilized to analyze the surface chemical compositions of the samples after 100 cycles. Inductively coupled plasma mass spectrometry (ICP-MS, iCAP7400) was applied to detect the TM content dissolved from the LRM cathode and deposited on the lithium anode. ^{19}F nuclear magnetic resonance (NMR) spectroscopy was performed using a 400 MHz NMR spectrometer (Bruker Avance II) with deuterated chloroform ($CDCl_3$) as the solvent. Time-of-flight secondary ion mass spectrometry (TOF-SIMS 5, ION-TOF GmbH) was carried out to detect the fragment information separated from the cathode surface. The testing principle is to use the primary pulse ions to bombard the sample surface, to determine the ion mass by measuring the flight time of the excited secondary ions, and then to obtain relevant surface information.

2.4. Theoretical calculations and MD simulations

The theoretical calculations were performed using density functional theory (DFT) with the Gaussian 09 software package. Molecular structures were optimized at the level of B3LYP/6-311G++(d,p), and GD3BJ was used for dispersion correction.[17–19] Acetone was used as the default solvent for the implicit solvent model (SMD), which has a similar dielectric constant to the carbonate electrolyte.[20] The electrostatic potential (ESP) and the Gibbs free energy (ΔG) representing the energy difference between products and reactants were also measured with the Gaussian 09.[21]

The GROMACS program with cubic periodic boundary conditions was used to perform molecular dynamic (MD) simulations.[22,23] The electrolyte simulation employed the General Amber Force Fields (GAFF), and the force field parameters were generated based on the sobtop. This force field was successfully applied in previous electrolyte studies.[24] The

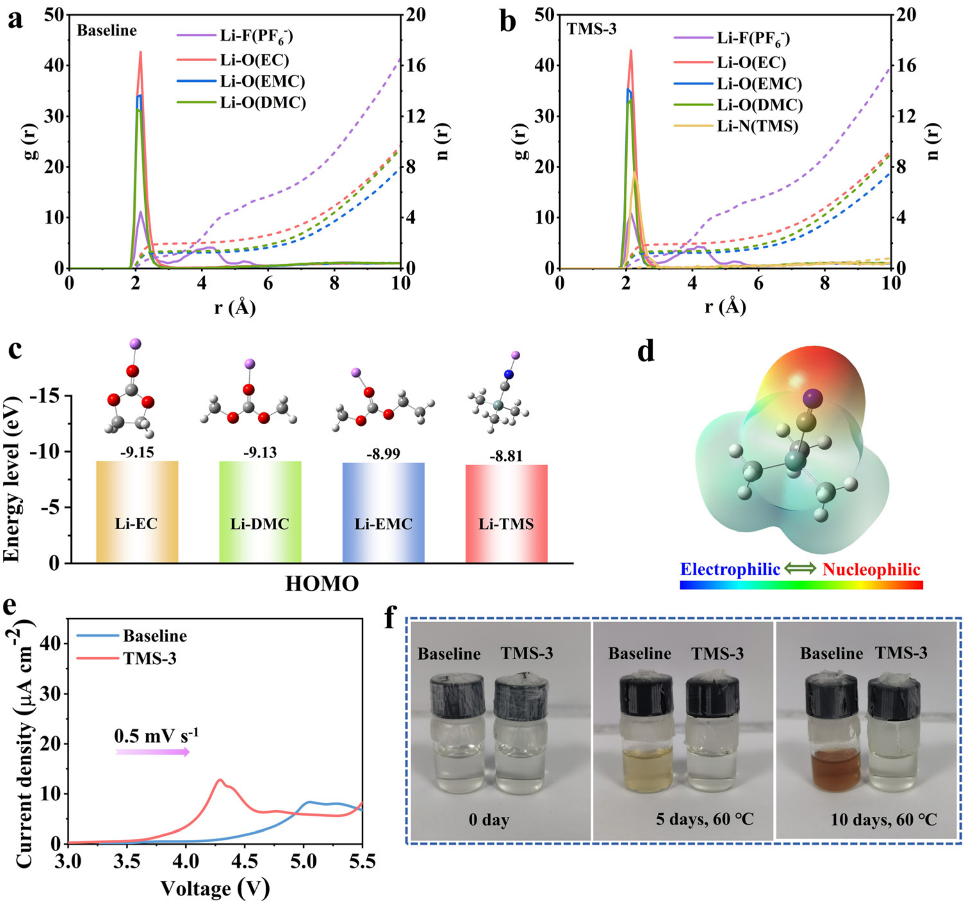

Fig. 1 Radial distribution function $g(r)$ and coordination number $n(r)$ of Li^+ calculated from MD simulations in the (a) baseline and (b) TMS-containing electrolytes. (c) Theoretical calculations of HOMO values for solvents and additive solvated with Li^+. (d) ESP charge distribution of TMS. (e) LSV tests at a scan rate of 0.5 mV s^{-1}. (f) High-temperature storage tests for the baseline and TMS-3 electrolytes at 60 °C.

Open Access Article. Published on 25 January 2025. Downloaded on 2/21/2025 12:54:23 PM.
This article is licensed under a Creative Commons Attribution-NonCommercial 3.0 Unported Licence.

packaging optimization for MD simulations (PACKMOL) tool was utilized to generate the initial atomic coordinate files for the MD simulations, guaranteeing a tightly packed starting configuration of the simulated system without any notable overlap between molecules.[25] A conjugate gradient energy minimization scheme (1.0×10^{-8}) for initialization configuration was used to minimize the unreasonable configurations in the initial structure. A 20 ns MD simulation was performed with the isothermal–isobaric ensemble (NPT) to confirm system equilibrium, followed by additional simulations of all atoms for 10 ns in the canonical ensemble (NVT). Visualization of the electrolyte structure was achieved using visual molecular dynamics (VMD).[26]

3. Results and discussion

3.1. Characterization of the electrolytes

Molecular dynamic (MD) simulations were carried out first to examine the impact of TMS on the solvation sheath of the carbonate electrolyte. Fig. 1a and b and Fig. S1 (ESI†) illustrate the radial distribution function, coordination number, and solvation model diagram of the electrolytes. A strong Li^+–N (TMS) peak appears near 0.22 nm in the TMS-containing electrolyte, indicating that the additive can participate in the formation of a solvation structure of Li^+ (Fig. 1b). The coordination numbers of Li^+-EC and Li^+-EMC in the baseline electrolyte are 1.97 and 1.24, respectively. With the introduction of TMS, these coordination numbers have decreased to some extent, which is advantageous for reducing polarization and forming a stable interface layer on the electrode surface.[27] The HOMO energies of TMS before and after solvation with Li^+ were computed by density functional theory (DFT), as shown in Fig. 1c and Fig. S2 (ESI†). The HOMO energy of the TMS molecule is close to EC before solvation, while the HOMO value of TMS solvated with Li^+ is calculated to be −8.81 eV, which is obviously higher than that of other solvents (−9.15 eV for EC, −9.13 eV for DMC, and −8.99 eV for EMC), indicating that TMS is more easily oxidized in the electrolyte. Moreover, an obvious oxidation peak at around 4.3 V is detected in the linear sweep voltammetry (LSV) tests, illustrating the priority decomposition of TMS (Fig. 1e).[15] According to the electrostatic potential (ESP) density distribution of TMS in Fig. 1d, the negative charges are mainly concentrated near the cyano (–CN) functional group. This distribution is attributed to the strong electron absorption property of the –CN group, which is conducive to the coordination between TMS and Li^+ and also provides the possibility for adsorbing on the cathode surface to participate in the CEI formation.[28,29]

Lithium hexafluorophosphate is prone to hydrolysis and lacks sufficient thermal stability, along with the generation of HF during long-term cycling, which poses a noticeable threat to the electrochemical performance of lithium batteries.[30] Therefore, it is important to remove HF and maintain the stability of the electrolyte. The Gibbs free energy (ΔG) of TMS reacting with HF was calculated using the DFT method, as illustrated in Fig. S3 (ESI†). The value of ΔG is -16.08 kcal mol^{-1}, which indicates that TMS can spontaneously combine with HF, and simultaneously accompanied by the breaking of the Si–C bond during the reaction process (also confirmed by XPS in Fig. 7f). Furthermore, after storing the baseline and TMS-containing electrolytes for 30 days, NMR tests are conducted to assess the efficacy of TMS in removing HF for purifying the electrolyte. As shown in Fig. S4 (ESI†), the signals near 75 ppm belong to PF_6^-, while the signals around 87 ppm are attributed to $P_xO_yF_z^-$ formed during the hydrolysis process of lithium salts.[31,32] It is worth noting that the signals of $P_xO_yF_z^-$ are stronger in the TMS-containing electrolyte, which may be due to the rightward shift of the hydrolysis equilibrium of lithium salts caused by the reaction of TMS with trace HF. Besides, a new peak can be observed at around 158 ppm in the TMS-containing electrolyte, resulting from the reaction between TMS and HF. The peak near 191 ppm is the characteristic peak of HF, which is not found after adding TMS, suggesting the positive role of TMS in clearing HF and purifying the electrolyte.[32,33]

In addition, the baseline and TMS-containing electrolytes were both put into the oven at the same time for high-temperature storage to accelerate the adverse reactions to compare their stability. As depicted in Fig. 1f, both electrolytes are initially clear and transparent. After 5 days of storage at 60 °C, the baseline electrolyte exhibits pale yellow, progressing to dark yellow after 10 days. This change may be related to the induction of solvent polymerization by HF and other decomposition products.[31] In comparison, the TMS-containing electrolyte still maintains transparency after 10 days. This clear distinction highlights the beneficial impact of the TMS additive on purifying the electrolyte, which is beneficial for enhancing the cycling performance of batteries.

3.2. Electrochemical performance of Li||LRM batteries

To confirm the optimal addition ratio, cycling performance was evaluated by assembling the Li||LRM batteries using the electrolytes with different amounts of TMS. As illustrated in Fig. S5 (ESI†), the battery using TMS-3 exhibits the best cycling performance, close to TMS-5. Considering that excessive additive will cause increased cost and may also lead to the formation of a thicker CEI that would increase the interfacial resistance and hinder the rapid migration of Li^+, the discussion in this work primarily focuses on the electrolyte with 3 wt% TMS (TMS-3).[20,34]

Long-term cycling differences between the baseline and TM-3 are displayed in Fig. 2a. The discharge capacity of the battery with the baseline electrolyte (baseline-battery) decreases to 169.5 mA h g^{-1} after 150 cycles at 1C, with a low capacity retention of 68.5%. In contrast, the higher discharge capacity of 224 mA h g^{-1} and capacity retention of 91% are maintained for the battery with TM-3 (TMS-battery) after 200 cycles under the same testing conditions. In addition, the average CE of the baseline-battery after 150 cycles is only 93.5%, while that of TMS-battery still exceeds 99.0% after 200 cycles (Fig. 2b). As shown in Fig. 2c, the voltage decay of the baseline-battery, especially after 100 cycles, is noticeably more serious, which

Open Access Article. Published on 25 January 2025. Downloaded on 2/21/2025 12:54:23 PM.
This article is licensed under a Creative Commons Attribution-NonCommercial 3.0 Unported Licence.

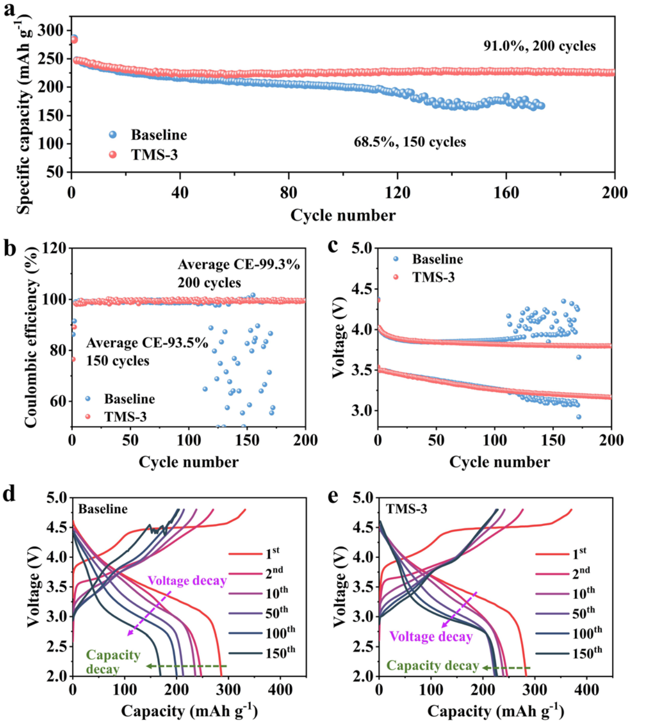

Fig. 2 (a) Cycling performance of Li||LRM batteries with the baseline and TMS-containing electrolytes between 2 and 4.8 V at 1C. (b) The comparison of coulombic efficiency in the two electrolytes. (c) Average charge and discharge voltages during cycling. (d) and (e) Charge and discharge curves of Li||LRM batteries (d) without and (e) with TMS.

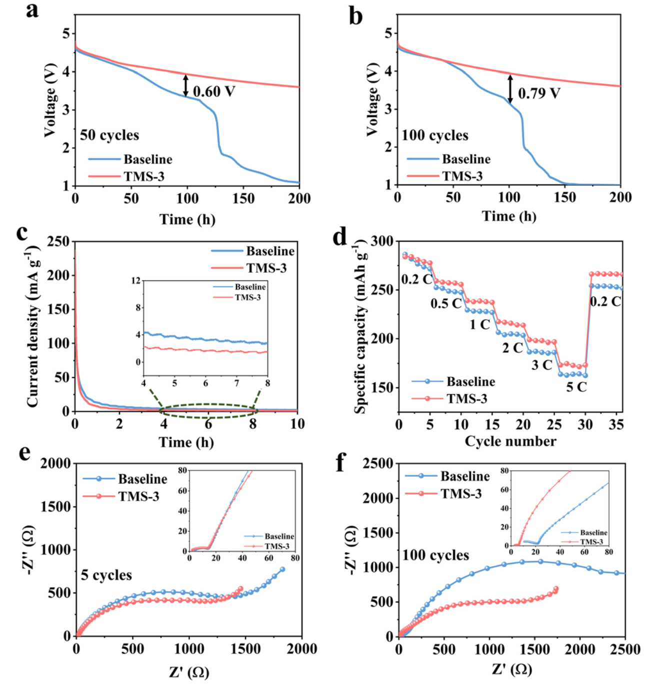

Fig. 3 (a) and (b) Self-discharge curves of Li||LRM batteries using different electrolytes at 4.8 V after (a) 50 and (b) 100 cycles. (c) Constant voltage floating charge test at 4.8 V in different electrolytes after 100 cycles. (d) Rate performance. (e) and (f) Nyquist plots of Li||LRM batteries in baseline and TMS-3 electrolytes after (e) 5 and (f) 100 cycles.

supports the beneficial effect of TMS on enhancing voltage stability. Fig. 2d and e display the galvanostatic charge–discharge curves of the batteries with different electrolytes, directly revealing a lower polarization and slower capacity degradation trend for the TMS-battery during long-term cycling. Moreover, the high-voltage stability of batteries is analyzed by the self-discharge and floating charge tests. As shown in Fig. 3a and b, the batteries with both two electrolytes can maintain a relatively stable voltage for the initial 50 hours after 50 and 100 cycles. However, after 50 hours, a noticeable voltage drop is observed for the baseline-battery compared to that with TMS-battery showing a considerably smaller decrease. The constant voltage floating charge test at 4.8 V also reflects a lower leakage current for the TMS-battery (Fig. 3c). These improvements are attributed to the stable and durable TMS-derived CEI film, which can effectively suppress the adverse interfacial side reactions under high voltage.

Furthermore, the influence of the TMS additive on the dynamic performance was analyzed through EIS, rate capability, and GITT tests. In the first five cycles, there is not much difference in the interface impedance R_f and charge transfer impedance R_{ct} in different electrolytes (Fig. 3e). Nevertheless, the overall impedance of the TMS-battery is notably smaller than that with the baseline electrolyte after 100 cycles (Fig. 3f). The results indicate that the uniform and stable CEI derived from TMS inhibits the severe decomposition of the electrolyte and the accumulation of byproducts on the cathode surface during long-term cycling, thus ensuring the Li^+ migration kinetics. The higher Li^+ diffusion coefficient in the GITT tests further confirms the positive effect of the TMS additive as shown in Fig. S6 (ESI†). Due to the reduced impedance and high ion diffusion coefficient during cycling, the transfer of Li^+ is accelerated. Consequently, the higher discharge capacities of 281, 257, 239, 216, 198 and 173 mA h g^{-1} can be achieved at 0.2, 0.5, 1, 2, 3 and 5C for the TMS battery, respectively (Fig. 3d and Fig. S7, ESI†).

In addition, the TMS-battery also exhibits superior cycling performance even when cycled at 3C. An initial discharge capacity of 163 mA h g^{-1} and a capacity retention of 81.2% are achieved after 300 cycles as shown in Fig. 4a. However, the capacity retention is reduced to 69.5% after only 150 cycles for the baseline battery at 3C. Moreover, the TMS-battery also exhibits a higher average CE of 99.3% and more stable average voltage (Fig. S8, ESI†). At low-temperature (−15 °C), although the general interface side reactions can be decreased to some extent, the polarization level will significantly increase, resulting in a slow diffusion rate and notable decrease in reversible capacity.[35] Owing to the high kinetic properties of TMS-derived CEI, the TMS-battery presents a higher discharge capacity of 123 mA h g^{-1} after 300 cycles at 0.33C, while the baseline-battery only retains 95 mA h g^{-1} (Fig. 4b). Fig. S9 (ESI†) further indicates that the voltage attenuation and capacity degradation have been well alleviated for the TMS-battery at low temperatures. Besides, the high-temperature cycling performance of the battery is also improved with the TMS-3 electrolyte

Open Access Article. Published on 25 January 2025. Downloaded on 2/21/2025 12:54:23 PM.
This article is licensed under a Creative Commons Attribution-NonCommercial 3.0 Unported Licence.

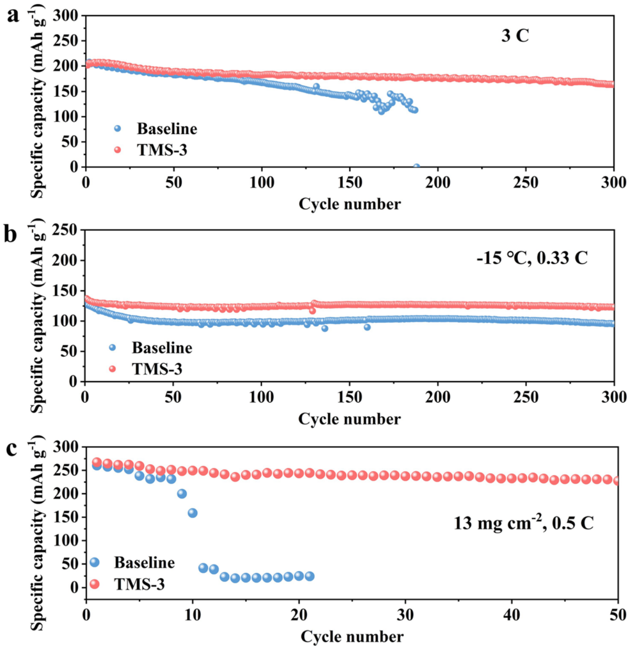

Fig. 4 Cycling performance with different electrolytes under various conditions at 2–4.8 V: (a) at 3C; (b) at 0.33C and −15 °C; (c) at 0.5C with a high mass loading of 13 mg cm^{-2}.

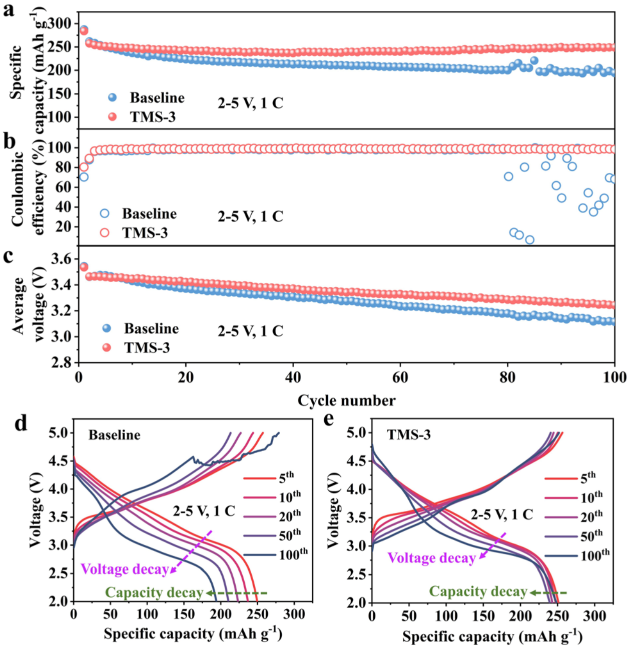

Fig. 5 Cycling performance of batteries with the two electrolytes at 2–5 V: (a) discharge capacity curves; (b) CE; (c) average discharge voltage; (d) and (e) charge and discharge curves (d) without and (e) with TMS.

(Fig. S10, ESI†). To further investigate the effect of the additive, cycling tests were carried out with a high cathode mass loading of ∼13 mg cm^{-2}. The results show that the TMS-battery still maintains a specific capacity of 227 mA h g^{-1} and exhibits 85% retention after 50 cycles at 0.5C, while the baseline-battery cannot exhibit normal charging and discharging behavior after just 10 cycles (Fig. 4c).

At higher voltages in the cycling process, the cathode materials will exhibit greater Li$^+$ intercalation/deintercalation depth and larger volume changes. Meanwhile, the electrolyte oxidation will also be stronger. These factors pose more rigorous requirements on the CEI film in terms of the mechanical strength, toughness, and resistance to strong oxidizing environments. In this regard, the upper cut-off voltage is increased to 5 V to explore the impact of the additive. As shown in Fig. 5a, the TMS-battery retains a high discharge capacity of 248 mA h g^{-1} after 100 cycles at 2–5 V, which is obviously better than that of the baseline-battery. The repeated occurrence of CEI rupture and repair at the local position on the cathode surface inevitably increases electrolyte consumption, causing CE to decrease and fluctuate significantly.[36,37] Therefore, the average CE of the baseline-battery within 100 cycles is only 90.5%, which is obviously lower than the 98.7% of TMS-battery (Fig. 5b). Further compared with the CE results over 100 cycles at 2–4.8 V in Fig. 2b, the CE of the baseline-battery decreases by 8.56% even though the upper cut-off voltage just increases by 0.2 V (4.8 to 5 V), while the TMS-battery only decreased by 0.48%. In addition, it can be seen from Fig. 5c–e that the voltage decay in the 2–5 V range has also been effectively relieved for the TMS-battery. These apparent differences in performance can be attributed to the multiple effects of the TMS additive. The cyano functional group in TMS promotes the formation of the complexes with TM–CN bonds on the LRM cathode surface, which helps to stabilize the layered structure and prevent corrosion from the electrolyte. Simultaneously, a uniform and durable CEI derived from the TMS-3 electrolyte separates the LRM cathode from the electrolyte, thereby alleviating interfacial side reactions and reducing the interfacial impedance. In addition, the trace HF in the electrolyte is also removed effectively by the TMS additive, benefitting suppressing the dissolution of TM. Resultantly, the long-term cycling performance of the LRM cathode is improved, which further highlights the application potential of TMS in high-voltage scenarios.

Meanwhile, considering that the lithium anode also affects the electrochemical performance, symmetrical batteries with the two electrolytes were constructed to evaluate the influence of the additive on the anode side. As illustrated in Fig. S11 (ESI†), cycling tests of Li||Li symmetrical batteries were performed at current densities of 0.5 and 1 mA cm^{-2}. The plating and stripping behaviors of Li$^+$ do not show significant differences, suggesting that the enhanced performance is mainly ascribed to the improvement of the cathode side.

3.3. Morphological and structural changes of LRM cathodes

During the high-voltage charging and discharging process, the decomposition of the electrolyte will lead to the generation of harmful products including HF, which would corrode the cathodes and cause the dissolution of TM. And under the influence of the electric field, the dissolved TM further migrates to and deposits on the surface of the lithium anode.[38] In the LRM cathode, the proportion of the Mn element is significantly

Open Access Article. Published on 25 January 2025. Downloaded on 2/21/2025 12:54:23 PM.
This article is licensed under a Creative Commons Attribution-NonCommercial 3.0 Unported Licence.

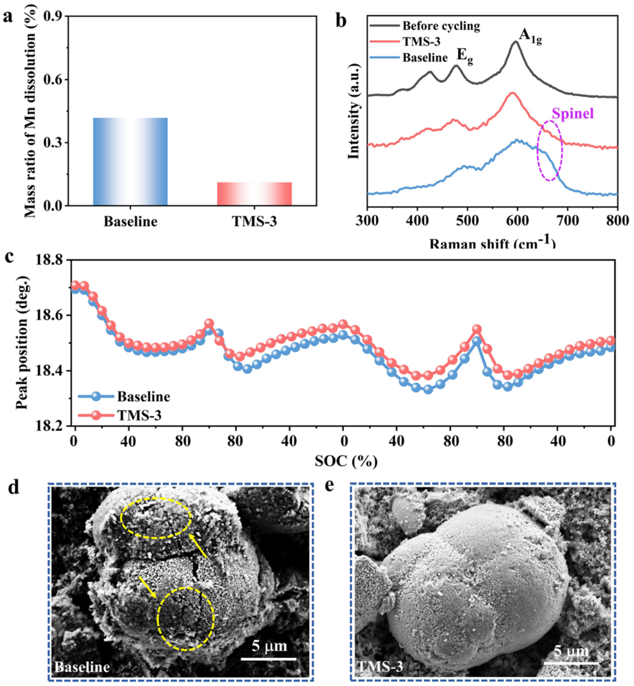

Fig. 6 (a) Mn dissolution after 100 cycles from the ICP test in the two electrolytes. (b) Raman spectra of cathodes before and after 100 cycles with different electrolytes. (c) *In situ* evolution of the (003) peak during the first two cycles at 0.5C. (d) and (e) SEM images of the cycled cathodes in the (d) baseline and (e) TMS-3 electrolytes.

higher, and the content of Mn deposited on the anode side can be used to reflect the extent of dissolution and destruction of the cathode structure. The batteries were disassembled after 100 cycles, and inductively coupled plasma (ICP) tests was carried out to determine the Mn content deposited on the anode side. As displayed in Fig. 6a. The TMS-battery displays a lower Mn content compared to that of the baseline-battery, which can be attributed to the positive role of TMS in stabilizing the cathode interface. After introducing TMS into the baseline electrolyte, the formed TM–CN complex and the durable CEI effectively avoid the direct contact between the cathode and adverse substances in the electrolyte, thus inhibiting TM dissolution.[39]

To deeply understand the difference in structural changes, the cycled cathodes with different electrolytes were tested by Raman spectroscopy. As shown in Fig. 6b, the E_g peak near 490 cm^{-1} corresponds to the bending vibration of the O–TM–O bond, while the A_{1g} peak at 600 cm^{-1} belongs to the stretching vibration of the TM–O bond.[40] The cathode matched with the baseline electrolyte shows a distinct characteristic peak of the spinel phase at 650 cm^{-1}.[41] In contrast, there is no notable change with the modified electrolyte, indicating the effects of TMS on stabilizing the layered structure of the LRM cathode. In addition, *in situ* XRD tests were performed to track the change of the (003) peak over the first two cycles. As shown in Fig. 6c, in the initial charging stage, the (003) peak shifts to a lower angle due to the extraction of Li$^+$ from the LiTMO$_2$ phase, causing greater electrostatic repulsion between the oxygen layers, thereby resulting in an increase in the lithium layer spacing. As the voltage gradually reaches around 4.5 V, the Li$_2$MnO$_3$ phase of the LRM cathode is activated and Li$^+$ is extracted from the TM layer, accompanied by the oxidation of the lattice oxygen. As a result, the (003) peak begins to shift towards the high angle. During the subsequent discharging process, Li$^+$ is re-inserted into the TM layer, causing the (003) peak to shift to the lower angle, followed by the shift to the high angle due to the reinsertion of Li$^+$ into the lithium layer. In the second cycle, the (003) peak shows similar evolution to that in the first cycle. Compared to the initial position, the (003) peak of the cathode with TMS-3 reveals a smaller average shift value of 0.170° (*vs.* baseline: 0.187°), suggesting that the variation of the cathode along the *c*-axis direction is partially inhibited. Besides, the (003) peak shift of cathode with TMS-3 is also smaller than that with baseline electrolyte after 100 cycles (Fig. S12, ESI†). This is attributed to the superior CEI formed from TMS-3, which is stable at high voltages and can effectively suppress unfavorable interface side reactions, reduce the consumption of active lithium, and ultimately maintain the stable cathode structure.

As illustrated in Fig. 6d and e, the cathode particle from the baseline-battery after 100 cycles exhibits a rough and uneven surface with irregular microcracks, while after the introduction of TMS, a relatively clean cathode surface is obtained and the whole structure is also maintained well. From the TEM results (Fig. 7a and b), it is evident that the CEI derived from the TMS-3 electrolyte presents a uniform and complete state, while the problems such as uneven thickness and poor local continuity appear for the CEI formed from the baseline electrolyte. The poor and uneven CEI would cause inconsistent lithiation of LRM cathode particles, exacerbating local stress accumulation and leading to particle cracking during cylcing.[28] The appearance of microcracks increases the contact area between the electrode and electrolyte, which accelerates adverse side reactions and the consumption of active lithium. As a result, issues such as continuous electrolyte oxidation and cathode structure deterioration occur, ultimately leading to rapid decline in electrochemical performance.

In order to further elucidate the enhanced mechanism in electrochemical performance of the LRM cathode with the TMS-3 electrolyte, the chemical compositions of the formed CEI layer were detected *via* X-ray photoelectron spectroscopy (XPS). As displayed in Fig. 7c-i, the P 1s XPS spectra exhibit two prominent peaks in the baseline and TMS-containing electrolytes, representing Li$_x$PO$_y$F$_z$ and LiP$_x$F$_y$ species, respectively.[42] In the O 1s XPS spectra, the peaks near 532 and 533.5 eV are assigned to the C═O and C–O species.[42,43] The components containing P are generated from the decomposition of lithium salts, while the C═O species primarily originate from the organic solvents in the electrolyte. The presence of stronger P-containing substances and C═O peaks in the baseline electrolyte suggests a more severe decomposition of lithium salts and organic solvents, which highlights the important effect of TMS in restraining the large consumption of the electrolyte. From the N 1s XPS spectra, it can be seen that there are two

Open Access Article. Published on 25 January 2025. Downloaded on 2/21/2025 12:54:23 PM.
This article is licensed under a Creative Commons Attribution-NonCommercial 3.0 Unported Licence.

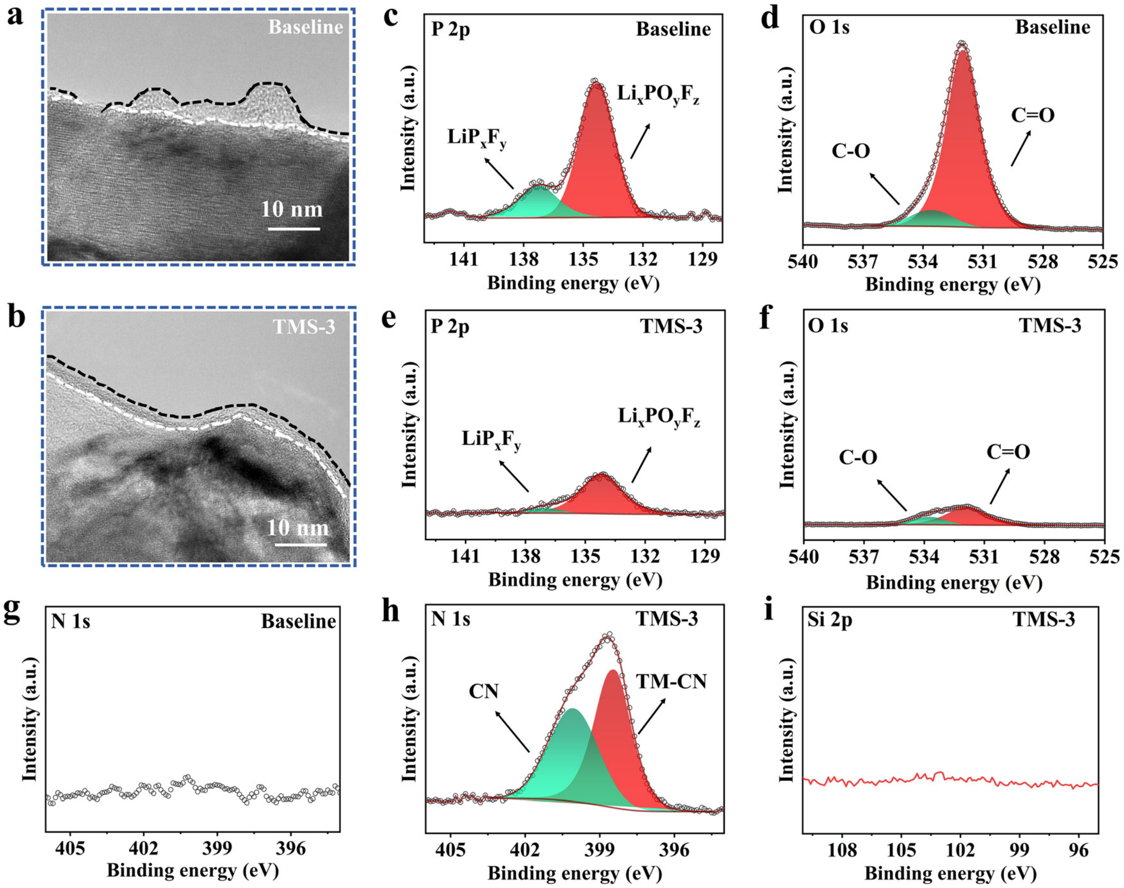

Fig. 7 TEM images of the cathodes after 100 cycles with the (a) baseline and (b) TMS-3 electrolytes. XPS spectra of the cycled cathodes in the (c), (d) and (g) baseline and (e), (f), (h) and (i) TMS-3 electrolytes.

obvious peaks of the TMS-containing electrolyte, corresponding to TM–CN and CN-containing species.[15,28,29] This is because the TMS additive has an electronegative cyano (-CN) functional group, and its strong coordination effect allows it to adsorb on the cathode surface to form the TM–CN adsorption layer, thereby stabilizing the LRM cathode interface.[15,44] Simultaneously, some –CN groups can further participate in the CEI formation and generate CN-containing species. Interestingly, no noticeable peak is observed in the Si 2p XPS spectra with the TMS-3 electrolyte, indicating that the Si–C bond of TMS is broken after the reaction and the Si-containing part may remain in the electrolyte and does not contribute to the CEI formation.

As shown in Fig. 8a–c and Fig. S13 (ESI†), the components of CEI after 100 cycles were further studied through the time-of-flight secondary ion mass spectrometry (TOF-SIMS). The fragment information of C_2HO^-, CH_2^-, and CH_3^- from the alkyl chain segments is generated during the decomposition of organic carbonate solvents. The higher intensity of these fragments confirms the severe decomposition of the baseline electrolyte (Fig. S13, ESI†). Moreover, significant fragments of CN^-, CNO^-, and $LiNC^-$ species are also detected for the LRM cathode with the TMS-containing electrolyte (Fig. 8a–c), which again indicates that the TMS additive is deeply involved in the formation process of CEI. Taking the N 1s XPS spectral test into account, the presence of CNO^- and $LiNC^-$ species suggests that some cyano groups are adsorbed on the LRM particle surface to construct the complex containing TM–CN bonds, while other cyano groups may undergo further reactions at the interface and become the components of the CEI. This behavior enriches the composition of the interface layer, which plays an important role in enhancing the stability of CEI, mitigating the electrolyte oxidation, and improving ionic diffusion.[15]

The above studies indicate that the introduction of TMS into the carbonate electrolyte can greatly improve the electrochemical performance of the LRM cathode, especially in the high-voltage range. The performance enhancement mechanism is outlined in Fig. 8d and e. On the one hand, TMS can purify the electrolyte through removing trace HF from the decomposition of the electrolyte. On the other hand, its electronegative cyano functional group can adsorb on the cathode surface to form a complex with TM–CN bonds to retain a stable cathode structure and reduce the surface degradation. Besides, the additive also contributes to the formation of the uniform and complete CEI with N-containing components, which is conducive to rapid Li^+ migration. This durable interfacial protective layer can also effectively avoid direct contact between the cathode and electrolyte, thus inhibiting the oxidative decomposition of the electrolyte and alleviating the dissolution of TMs.

Open Access Article. Published on 25 January 2025. Downloaded on 2/21/2025 12:54:23 PM.
This article is licensed under a Creative Commons Attribution-NonCommercial 3.0 Unported Licence.

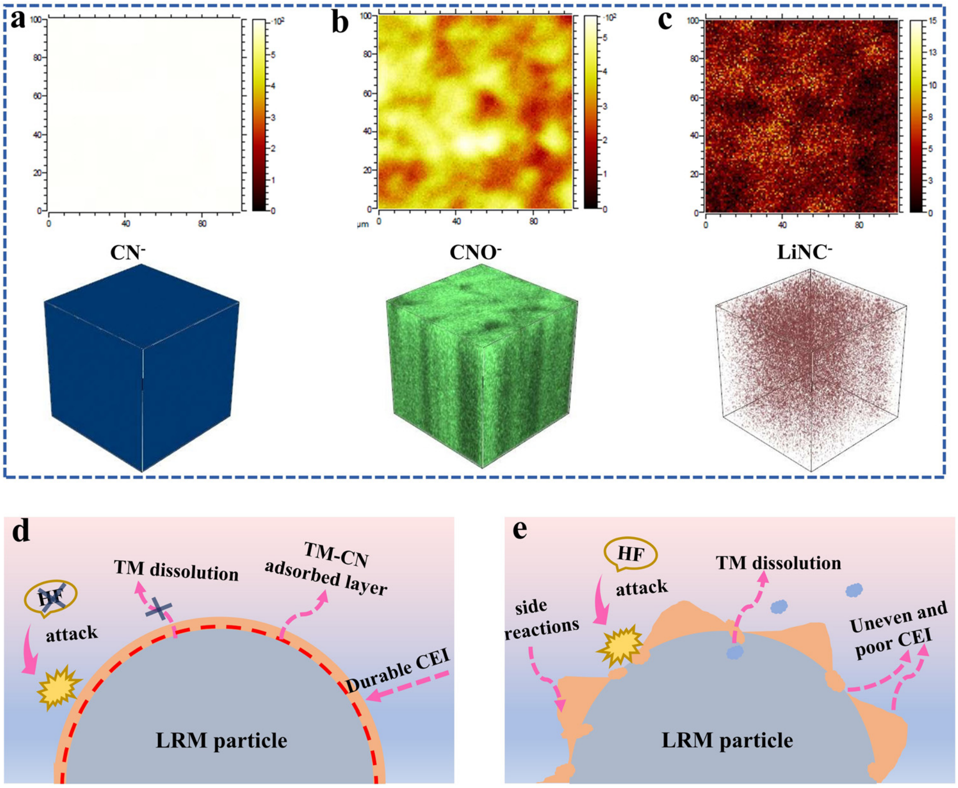

Fig. 8 (a)–(c) TOF-SIMS 3D and 2D render images of fragments on the cycled cathodes with the TMS-3 electrolyte: (a) CN^- (as shown on the adjacent ruler, bright white color represents a high content); (b) CNO^-; (c) $LiNC^-$; (d) and (e) schematic illustrations of the performance improvement mechanism by (d) the baseline electrolyte and (e) the TMS-3 electrolyte.

4. Conclusions

In summary, the unique silane additive with a cyano functional group has been successfully used to improve the high-voltage performance of the carbonate electrolyte. The introduced TMS additive can participate in CEI formation to obtain a low-resistance and durable CEI with N-rich components, reducing side reactions of the electrolyte in a high-voltage environment. By combining with the electronegative cyano groups to form the complex containing TM–CN bonds on the cathode surface, the oxidative decomposition of the electrolyte and destruction of the cathode structure can be greatly alleviated. In addition, the reaction between TMS and HF can also effectively reduce the content of harmful substances in the electrolyte. Therefore, the cycling stability of the LRM cathode has been well maintained. The battery with 3 wt% TMS in the electrolyte displays a high discharge capacity of 224 mA h g^{-1} with a retention over 90% after 200 cycles at 1C. Even under high mass loading of 13 mg cm^{-2}, a discharge capacity of 227 mA h g^{-1} and an 85% capacity retention are achieved after 50 cycles at 0.5C. Furthermore, the rate performances have also been significantly improved with the optimized electrolyte. This work presents a practical approach to improve the electrochemical performance of LRM cathodes by introducing a functional additive to remove harmful acidic substances in the electrolyte while stabilizing the electrode interface.

Author contributions

Dongwei Zhou: conceptualization, methodology, formal analysis, investigation, data curation, and writing – original draft. Shihao Wang, Guiyang Gao, Jie Zhu, Chengkun Zhang, and Saichao Li: investigation, formal analysis, validation, and writing – review & editing. Zhanlin Yang and Baisheng Sa: resources, software, visualization, and writing – review & editing. Jie Lin, Dong-Liang Peng, and Qingshui Xie: funding acquisition, project administration, resources, supervision, and writing – review & editing.

Data availability

The data supporting this article can be found in the ESI.†

Conflicts of interest

The authors have no conflicts to declare.

Acknowledgements

The work received financial support from the National Natural Science Foundation of China (Grant No. 52272240, 51931006, U22A20118, 52431009 and 52101273), the Science and Technology Planning Projects of Fujian Province of China

Open Access Article. Published on 25 January 2025. Downloaded on 2/21/2025 12:54:23 PM.
This article is licensed under a Creative Commons Attribution-NonCommercial 3.0 Unported Licence.

(Grant No. 2023H0003), the Fundamental Research Funds for the Central Universities of China (Xiamen University: No. 20720220074 and 20720240053), and the ''Double-First Class'' Foundation of Materials Intelligent Manufacturing Discipline of Xiamen University. Financial support from the IEST (Initial Energy Science and Technology) (No. 20223160A0088) is also gratefully acknowledged.

References

1 K. Kim, H. Ma, S. Park and N.-S. Choi, Electrolyte-additive-driven interfacial engineering for high-capacity electrodes in lithium-ion batteries: promise and challenges, *ACS Energy Lett.*, 2020, **5**, 1537–1553.

2 H. Zheng, X. Han, W. Guo, L. Lin, Q. Xie, P. Liu, W. He, L. Wang and D.-L. Peng, Recent developments and challenges of Li-rich Mn-based cathode materials for high-energy lithium-ion batteries, *Mater. Today Energy*, 2020, **18**, 100518.

3 X. Qi, Q. Dong, H. Dong, B. Hou, H. Liu, N. Shang, S. Zhang, L. Wang, H. Shao, Y. Shen, S. Chen and X. Zhao, Copper-induced lattice distortion in $Na_4Fe_3(PO_4)_2(P_2O_7)$ cathode enabling high power density Na-ion batteries with good cycling stability, *Energy Storage Mater.*, 2024, **73**, 103861.

4 R. Zhu, J. Wang and J. Li, $Li_4Mn_5O_{12}$ Cathode for Both 3 V and 4 V Lithium-ion Batteries, *Chem. Res. Chin. Univ.*, 2021, **37**, 1031–1043.

5 S. Wang, J. Suo, Y. Liu, W. Guo, G. Gao, X. Han, M. Fan, R. Wu, D.-L. Peng and Q. Xie, Enhancing the electrochemical properties of Li-rich layered oxide cathodes by a facile Fe/Ti integrated modification strategy, *Chem. Eng. J.*, 2024, **497**, 154387.

6 J. G. Han, S. J. Lee, J. Lee, J. S. Kim, K. T. Lee and N. S. Choi, Tunable and robust phosphite-derived surface film to protect lithium-rich cathodes in lithium-ion batteries, *ACS Appl. Mater. Interfaces*, 2015, **7**, 8319–8329.

7 J.-G. Han, J. B. Lee, A. Cha, T. K. Lee, W. Cho, S. Chae, S. J. Kang, S. K. Kwak, J. Cho, S. Y. Hong and N.-S. Choi, Unsymmetrical fluorinated malonatoborate as an amphoteric additive for high-energy-density lithium-ion batteries, *Energy Environ. Sci.*, 2018, **11**, 1552–1562.

8 J. G. Han, C. Hwang, S. H. Kim, C. Park, J. Kim, G. Y. Jung, K. Baek, S. Chae, S. J. Kang, J. Cho, S. K. Kwak, H. K. Song and N. S. Choi, An Antiaging Electrolyte Additive for High-Energy-Density Lithium-Ion Batteries, *Adv. Energy Mater.*, 2020, **10**, 2000563.

9 W. Guo, Y. Zhang, L. Lin, Y. Liu, M. Fan, G. Gao, S. Wang, B. Sa, J. Lin, Q. Luo, B. Qu, L. Wang, J. Shi, Q. Xie and D. L. Peng, Regulation of Interfacial Lattice Oxygen Activity by Full-Surface Modification Engineering towards Long Cycling Stability for Co-Free Li-Rich Mn-Based Cathode, *Small*, 2023, **19**, 2300175.

10 C.-C. Su, M. He, P. C. Redfern, L. A. Curtiss, I. A. Shkrob and Z. Zhang, Oxidatively stable fluorinated sulfone electrolytes for high voltage high energy lithium-ion batteries, *Energy Environ. Sci.*, 2017, **10**, 900–904.

11 Y. Li, W. Li, R. Shimizu, D. Cheng, H. Nguyen, J. Paulsen, S. Kumakura, M. Zhang and Y. S. Meng, Elucidating the Effect of Borate Additive in High-Voltage Electrolyte for Li-Rich Layered Oxide Materials, *Adv. Energy Mater.*, 2022, **12**, 2103033.

12 H. Liu, A. J. Naylor, A. S. Menon, W. R. Brant, K. Edström and R. Younesi, Understanding the Roles of Tris (trimethylsilyl) Phosphite (TMSPi) in $LiNi_{0.8}Mn_{0.1}Co_{0.1}O_2$ (NMC811)/Silicon-Graphite (Si-Gr) Lithium-Ion Batteries, *Adv. Mater. Interfaces*, 2020, **7**, 2000277.

13 X. Wu, Z. Wang, X. Li, H. Guo, Y. Zhang and W. Xiao, Effect of lithium difluoro(oxalato)borate and heptamethyldisilazane with different concentrations on cycling performance of $LiMn_2O_4$, *J. Power Sources*, 2012, **204**, 133–138.

14 A. S. Wotango, W.-N. Su, E. G. Leggesse, A. M. Haregewoin, M.-H. Lin, T. A. Zegeye, J.-H. Cheng and B.-J. Hwang, Improved Interfacial Properties of MCMB Electrode by 1-(Trimethylsilyl)imidazole as New Electrolyte Additive To Suppress $LiPF_6$ Decomposition, *ACS Appl. Mater. Interfaces*, 2017, **9**, 2410–2420.

15 Z. Ren, H. Qiu, C. Fan, S. Zhang, Q. Zhang, Y. Ma, L. Qiao, S. Wang, G. Xu, Z. Cui and G. Cui, Delicately Designed Cyano-Siloxane as Multifunctional Additive Enabling High Voltage $LiNi_{0.9}Co_{0.05}Mn_{0.05}O_2$/Graphite Full Cell with Long Cycle Life at 50 °C, *Adv. Funct. Mater.*, 2023, **33**, 2302411.

16 Y. Ji, S. Li, G. Zhong, Z. Zhang, Y. Li, M. J. McDonald and Y. Yang, Synergistic Effects of Suberonitrile-LiBOB Binary Additives on the Electrochemical Performance of High-Voltage $LiCoO_2$ Electrodes, *J. Electrochem. Soc.*, 2015, **162**, A7015–A7023.

17 X. Zhang, G. Liu, K. Zhou, T. Jiao, Y. Zou, Q. Wu, X. Chen, Y. Yang and J. Zheng, Enhancing cycle life of nickel-rich $LiNi_{0.9}Co_{0.05}Mn_{0.05}O_2$ via a highly fluorinated electrolyte additive – pentafluoropyridine, *Energy Mater.*, 2021, **1**, 100005.

18 Y. Jie, X. Liu, Z. Lei, S. Wang, Y. Chen, F. Huang, R. Cao, G. Zhang and S. Jiao, Enabling High-Voltage Lithium Metal Batteries by Manipulating Solvation Structure in Ester Electrolyte, *Angew. Chem., Int. Ed.*, 2020, **59**, 3505–3510.

19 Y. Rao, Y. Lu, L. Zhang, S. Ju, N. Yu, A. Zhang, L. Chen and H. Wang, A metadata schema for lattice thermal conductivity from first-principles calculations, *J. Mater. Inf.*, 2022, **2**, 17.

20 A. Fu, J. Lin, J. Zheng, D.-Y. Wu, Z. Zhang, P. Yan, Y. Su, C. Xu, J. Hao, H. Zheng, H. Duan, Y. Ding, J. Yan, S. Huang, C. Liu, C. Tang, X. Fang and Y. Yang, Additive evolved stabilized dual electrode-electrolyte interphases propelling the high-voltage Li||$LiCoO_2$ batteries up to 4.7 V, *Nano Energy*, 2024, **119**, 109095.

21 Y. Li, M. Liu, K. Wang, C. Li, Y. Lu, A. Choudhary, T. Ottley, D. Bedrov, L. Xing and W. Li, Single-Solvent-Based Electrolyte Enabling a High-Voltage Lithium-Metal Battery with Long Cycle Life, *Adv. Energy Mater.*, 2023, **13**, 2300918.

Open Access Article. Published on 25 January 2025. Downloaded on 2/21/2025 12:54:23 PM.
This article is licensed under a Creative Commons Attribution-NonCommercial 3.0 Unported Licence.

22 M. J. Abraham, T. Murtola, R. Schulz, S. Páll, J. C. Smith, B. Hess and E. Lindahl, GROMACS: High performance molecular simulations through multi-level parallelism from laptops to supercomputers, *SoftwareX*, 2015, **1–2**, 19–25.

23 Y. Liu, Y. Lin, Z. Yang, C. Lin, X. Zhang, S. Chen, G. Hu, B. Sa, Y. Chen and Y. Zhang, Stable Harsh-Temperature Lithium Metal Batteries Enabled by Tailoring Solvation Structure in Ether Electrolytes, *ACS Nano*, 2023, **17**, 19625–19639.

24 Y. Wu, A. Wang, Q. Hu, H. Liang, H. Xu, L. Wang and X. He, Significance of Antisolvents on Solvation Structures Enhancing Interfacial Chemistry in Localized High-Concentration Electrolytes, *ACS Cent. Sci.*, 2022, **8**, 1290–1298.

25 L. Martínez, R. Andrade, E. G. Birgin and J. M. Martínez, PACKMOL: A package for building initial configurations for molecular dynamics simulations, *J. Comput. Chem.*, 2009, **30**, 2157–2164.

26 W. Humphrey, A. Dalke and K. Schulten, VMD: Visual molecular dynamics, *J. Mol. Graphics*, 1996, **14**, 33–38.

27 Z. Lu, D. Liu, K. Dai, K. Liu, C. Jing, W. He, W. Wang, C. Zhang and W. Wei, Tailoring solvation chemistry in carbonate electrolytes for all-climate, high-voltage lithium-rich batteries, *Energy Storage Mater.*, 2023, **57**, 316–325.

28 M. Mao, L. Gong, X. Wang, Q. Wang, G. Zhang, H. Wang, W. Xie, L. Suo and C. Wang, Electrolyte design combining fluoro- with cyano- substitution solvents for anode-free Li metal batteries, *Proc. Natl. Acad. Sci. U. S. A.*, 2024, **121**, e2316212121.

29 X. Yang, M. Lin, G. Zheng, J. Wu, X. Wang, F. Ren, W. Zhang, Y. Liao, W. Zhao, Z. Zhang, N. Xu, W. Yang and Y. Yang, Enabling Stable High-Voltage $LiCoO_2$ Operation by Using Synergetic Interfacial Modification Strategy, *Adv. Funct. Mater.*, 2020, **30**, 2004664.

30 C. Ye, W. Tu, L. Yin, Q. Zheng, C. Wang, Y. Zhong, Y. Zhang, Q. Huang, K. Xu and W. Li, Converting detrimental HF in electrolytes into a highly fluorinated interphase on cathodes, *J. Mater. Chem. A*, 2018, **6**, 17642–17652.

31 Y. Zou, K. Zhou, G. Liu, N. Xu, X. Zhang, Y. Yang, J. Zhang and J. Zheng, Enhanced Cycle Life and Rate Capability of Single-Crystal, Ni-Rich $LiNi_{0.9}Co_{0.05}Mn_{0.05}O_2$ Enabled by 1,2,4-1H-Triazole Additive, *ACS Appl. Mater. Interfaces*, 2021, **13**, 16427–16436.

32 J. Lan, Q. Zheng, H. Zhou, J. Li, L. Xing, K. Xu, W. Fan, L. Yu and W. Li, Stabilizing a High-Voltage Lithium-Rich Layered Oxide Cathode with a Novel Electrolyte Additive, *ACS Appl. Mater. Interfaces*, 2019, **11**, 28841–28850.

33 H. Zhu, Y. Zhang, M. Li, J. Luo, W. Wei and S. Zhang, Constructing a stable interface by 2,4,6-trimethoxyboroxine as an electrolyte additive for Li-rich layered oxide cathode under high voltage, *J. Electroanal. Chem.*, 2021, **899**, 115682.

34 W.-C. Zheng, C.-G. Shi, P. Dai, Z. Huang, J.-X. Lin, H. Chen, M.-L. Sun, C.-H. Shen, C.-X. Luo, Q. Wang, X. Feng, Y.-M. Wei, L. Huang and S.-G. Sun, A functional electrolyte additive enabling robust interphases in high-voltage $Li||LiNi_{0.8}Co_{0.1}Mn_{0.1}O_2$ batteries at elevated temperatures, *J. Mater. Chem. A*, 2022, **10**, 21912–21922.

35 S. Li, Y. Liu, Y. Zhang, W. He, H. Zheng, W. Guo, H. Wu, G. Gao, B. Sa, L. Wang, Q. Xie, J. Lin, J. Shi and D.-L. Peng, Interfacial oxygen coordination environment regulation towards high-performance Li-rich layered oxide cathode, *Chem. Eng. J.*, 2023, **462**, 142194.

36 B. Zhang, X. Wu, H. Luo, H. Yan, Y. Chen, S. Zhou, J. Yin, K. Zhang, H.-G. Liao, Q. Wang, Y. Zou, Y. Qiao and S.-G. Sun, Gradient Interphase Engineering Enabled by Anionic Redox for High-Voltage and Long-Life Li-Ion Batteries, *J. Am. Chem. Soc.*, 2024, **146**, 4557–4569.

37 D. Wu, C. Zhu, H. Wang, J. Huang, G. Jiang, Y. Yang, G. Yang, D. Tang and J. Ma, Mechanically and Thermally Stable Cathode Electrolyte Interphase Enables High-temperature, High-voltage $Li||LiCoO_2$ Batteries, *Angew. Chem., Int. Ed.*, 2024, **63**, e202315608.

38 R. Sim, L. Su, A. Dolocan and A. Manthiram, Delineating the Impact of Transition-Metal Crossover on Solid-Electrolyte Interphase Formation with Ion Mass Spectrometry, *Adv. Mater.*, 2023, **36**, 2311573.

39 J. T. Zhao, X. Zhang, Y. Liang, Z. J. Han, S. Q. Liu, W. Q. Chu and H. J. Yu, Interphase Engineering by Electrolyte Additives for Lithium-Rich Layered Oxides: Advances and Perspectives, *ACS Energy Lett.*, 2021, **6**, 2552–2564.

40 B. Jiang, J. Li, B. Luo, Q. Yan, H. Li, L. Liu, L. Chu, Y. Li, Q. Zhang and M. Li, $LiPO_2F_2$ electrolyte additive for high-performance Li-rich cathode material, *J. Energy Chem.*, 2021, **60**, 564–571.

41 W. He, P. Liu, B. Qu, Z. Zheng, H. Zheng, P. Deng, P. Li, S. Li, H. Huang, L. Wang, Q. Xie and D. L. Peng, Uniform Na^+ Doping-Induced Defects in Li-and Mn-Rich Cathodes for High-Performance Lithium-Ion Batteries, *Adv. Sci.*, 2019, **6**, 1802114.

42 H. Q. Pham, M. Mirolo, M. Tarik, M. El Kazzi and S. Trabesinger, Multifunctional electrolyte additive for improved interfacial stability in Ni-rich layered oxide full-cells, *Energy Storage Mater.*, 2020, **33**, 216–229.

43 B. Zhang, L. Wang, X. Wang, S. Zhou, A. Fu, Y. Yan, Q. Wang, Q. Xie, D. Peng, Y. Qiao and S.-G. Sun, Sustained releasing superoxo scavenger for tailoring the electrode-electrolyte interface on Li-rich cathode, *Energy Storage Mater.*, 2022, **53**, 492–504.

44 J. Zhao, Y. Liang, X. Zhang, Z. Zhang, E. Wang, S. He, B. Wang, Z. Han, J. Lu, K. Amine and H. Yu, In Situ Construction of Uniform and Robust Cathode-Electrolyte Interphase for Li-Rich Layered Oxides, *Adv. Funct. Mater.*, 2020, **31**, 2009192.